DEVELOPMENT OF A TWO-SCALE INCREMENTAL MODEL FOR MULTIAXIAL FATIGUE IN AN INDUSTRIAL CONTEXT

R. Desmorat[a], A. du Tertre[b], G. Barbier[a]

a LMT Cachan, 94235 Cachan, France

b Snecma, Space Engines Division, 27200 Vernon, France

Abstract. Since 2005 a complete development program based on the LMT incremental two-scale Model for fatigue life prediction in multiaxial high cycle fatigue has been conducted by the Space Engine Division of Snecma in order to cope with multiaxial high stress ratios loadings applied on components, eventually locally plastified. This project went through an evaluation phase followed by improvement works and finally a validation approach implying several multiaxial fatigue tests campaigns on different materials.
This article aims at summarizing the principal theoretical evolutions of the model obtained during this development program.
Thus, a first evaluation of the model prediction performances on a batch of titanium alloy notched specimens at low temperature allowed to identify different improvement axis. Among them, the implementation of Drücker-Prager term into the plastic criterion function (Barbier & al. 2009 [42]) was a significant one. It allowed to improve the model's ability to take the mean stress effect into account.
Since then, the model has been evaluated on different bi-axial tests and appeared to be easy to use and identify thanks to the associate DAMAGE 2010 post-processor software.

1. INTRODUCTION

In the frame of its rocket engines design and development activities, the Space Engine Division of Snecma has to deal with complex fatigue phenomena on metallic components. Indeed, some of these parts can be subjected to multiaxial fatigue at a high number of cycles (i.e. N cycles > 1.10^5) under high stress ratios. Nevertheless, negative stress ratios can also be observed as well as locally plastified areas. These aspects imply to be able to correctly predict the fatigue life by means of a relevant and validated multiaxial model which efficiently takes the mean stress effect into account as well as plasticity at macroscale.

For that purpose, Snecma launched in 2005 a research project in partnership with Cnes and LMT based on the LMT incremental two-scale model [28] and its associated post-processor DAMAGE [26], [37]. This pluri-annual project aimed not only at evaluating this model but also at improving and finally validating it. The final goal was of course to be able to answer industrial needs in a design office context. The industrial aspect of this model and associated methodologies and tools was of utmost importance. Indeed, the possibility to have an easy method to identify the model using a limited amount of experimental values and then the possibility to rapidly use the model in the design office were the main challenges to fulfil.

Considering these requirements the incremental two-scale model proposed by the LMT appeared to offer the qualities and the evolution potential necessary to take the main influent phenomena encountered in high cycle fatigue into account. The two-scale model belongs to the incremental models family and is based on the Continuum Damage Mechanics developed at LMT Cachan by Lemaitre and coworkers since the beginning of the eighty's [16] [18].

At the beginning of the project priority was set on the multiaxiality aspect and on the mean stress effect, but of course, the improvements and results obtained can lead to further developments.

This article presents the main phases of the project and summarizes the main theoretical evolutions of the model since the beginning of these activities.

2. THE INDUSTRIAL PROJECT

The project was divided into three main phases:

- Phase 1: Evaluation of the existing two-scale model in its 2005 formulation and definition of improvements axis,
- Phase 2: Improvements implementation,
- Phase 3: Validation of the "new" two-scale model on HCF multiaxial tests,

These activities were partially carried out at Snecma's center of Vernon but also principally at LMT Cachan laboratory. Phase 3 was also carried out with other industrial partners : EDF and Areva NP during the Barbier Ph-D thesis (2006-2009) [42]. Different material were used, mainly titanium and nickel alloys.

3. MODEL'S INITIAL FORMULATION (2005)

3.1. Specificity

Fatigue is often addressed with stress amplitude closed form expressions, i.e. laws directly relating the stress amplitude to the number of cycles to failure or to crack initiation (Basquin, 1910; Manson et al, 1964; Aas-Jackobsen and Lenshow, 1973; Leiholz, 1986; Fatemi and Yang, 1998 ([1] to [5])). The mean stress effect is then simply modelled by the introduction in previous law, as a parameter, of the stress ratio $R\sigma = \sigma min/\sigma max$ (minimum stress divided by the maximum stress over a cycle). The difficulty is then to extend such a modelling to 3D cases and to non-cyclic loading conditions (Smith et al, 1970; Brown and Miller, 1973; Dang Van, 1973; Hua and Socie, 1984; Dang Van, 1993; Papadopoulos, 1995; Papadopoulos et al, 1997; Nicholas, 1999; Morel, 2000 ([6] to [14]).

On the other hand, Continuum Damage Mechanics, naturally a 3D modelling, can also be used for fatigue (Lemaitre and Chaboche, 1974; Lemaitre and Plumtree, 1979; Chaboche and Lesne, 1988, [15] to [17]). The cyclic relationships are gained firstly from the time integration over one cycle of the damage and constitutive laws, and secondly from the integration over the whole loading (Lemaitre, 1992; Paas et al, 1993; Desmorat, 2006; Flacelière et al., 2007 ([18] to [21])).

The introduction of the stress ratio is then not natural and may become a difficult task. A first possibility is to model the microdefects or microcracks closure effect (also called quasi-unilateral condition (Ladevèze and Lemaitre, 1984; Lemaitre, 1992; Chaboche, 1993; Desmorat et al, 2007) and its coupling with damage growth (Desmorat and Cantournet, 2008 [25]). With this in mind and with the additional fact that HCF most often corresponds to fatigue in the elastic regime, an incremental two-scale damage model has been proposed with good abilities for fatigue (Lemaitre and Doghri, 1994; Lemaitre et al, 1999; Desmorat and Lemaitre, 2001 ([26] to [28]).

3.2. Principle

On the remark that High Cycle Fatigue, either thermally or mechanically activated, occurs for an elastic regime at the RVE scale, the mesoscale of continuum mechanics, a twoscalesdamage model has been built (Lemaitre and Doghri, 1994 [26]; Lemaitre et al, 1999 [27]; Desmorat and Lemaitre, 2001; Desmorat et al, 2007; Sauzay, 2000 ([28] to [30])). It accounts for micro-plasticity and micro-damage at the defects scale or microscale. The mo del is phenomenological, describing micro-plasticity with classical 3D von Mises plasticity equations, describing micro-damage by Lemaitre (Lemaitre, 1992; Lemaitre and Chaboche, 1985) damage evolution law $\dot{D} = \left(\frac{Y}{S}\right)^s \dot{p}$ of damage governed by the accumulated plastic strain rate $\dot{p}$ and enhanced by the strain energy density (denoted Y as the thermodynamics force associated with the damage variable D). Parameters S and s are material and temperature dependent. A scale transition law such as Eshelby-Kröner localization law makes the link between both mesoscopic and microscopic scales.

The general principles initially followed for building a two-scale damage model for complex fatigue applications are as follows (Fig. 1).

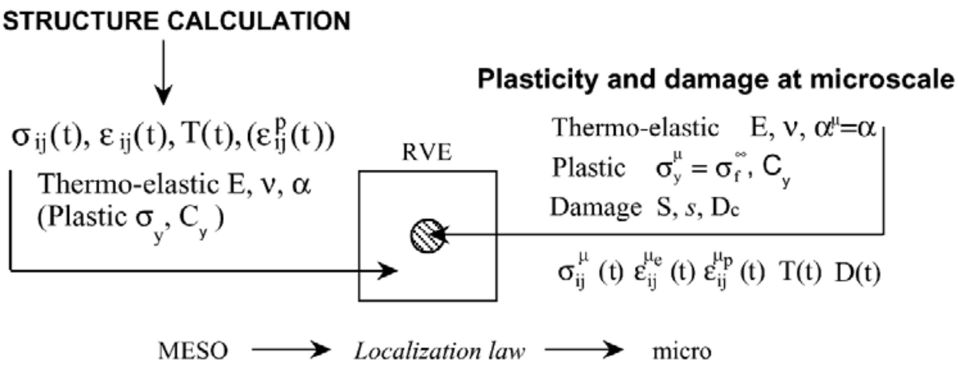

Figure 1: Micro element imbedded in a thermo-elastic Representative Volume Element.

- At the mescocale, the scale of the RVE of continuum mechanics, the behavior is considered as (thermo)-elastic, the material yield stress σy being usually not reached in HCF (accordingly called elastic fatigue).
- At the microscale which is the defects scale, defects conceptually gathered as a weak inclusion imbedded in the previous RVE. The behavior at microscale is (thermo-)elasto-plasticity coupled with damage, the weakness of the inclusion being represented by a yield stress at microscale $\sigma^\mu{}_y < \sigma_y$ taken equal to the asymptotic fatigue limit of the material $\sigma_f{}^\infty$ @ $R_\sigma = -1$.

At the mesoscale, the stresses are denoted σ, the total, elastic and plastic strains ε, εe, εp. They are known from an elasto-plastic Finite Element computation. An initial hardening can be handled by the two-scale damage model by considering constant non zero mesoscopic plastic strains ε_p -- for instance gained from the nonlinear FE analysis of the initial yielding.

The values at the microscale have an upper-script μ. For High Cycle Fatigue, with plasticity and damage assumed to occur at the microscale only, one has $\varepsilon_p^\mu \neq 0$, $0 < D < 1$, where for simplicity, the damage variable at the microscale has no upper-script ($D = D^\mu$).

3.3. Thermo-elastic behaviour at mesoscale

The thermoelastic law for the RVE reads :

$$\boldsymbol{\epsilon}^e = \frac{1+\nu}{E}\boldsymbol{\sigma} - \frac{\nu}{E}\mathrm{tr}\,\boldsymbol{\sigma}\,\mathbf{1} + \alpha(T - T_{\mathrm{ref}})\mathbf{1} \tag{1}$$

with E the Young modulus, ν the Poisson ratio, α the thermal expansion coefficient and T_{ref} the reference temperature. The non homogeneous temperature and eventually time dependent field in a structure T(x,t) is usually determined from an initial heat transfer computation. The mechanical properties E, ν , α may depend on the temperature. The shear and bulk modulus of the material will respectively be $G = E/2(1+\nu)$ and $K = E/3(1-2\nu)$.

3.4. Plasticity and damage at microscale

A law of thermo-elasto-plasticity coupled with damage is considered at microscale. No viscosity is considered as for the applications in mind the temperature will remain much lower than one third of the melting temperature. The elasticity law reads then (recall that μ-upperscript stands for "variable at microscale"):

$$\boldsymbol{\epsilon}^{\mu e} = \frac{1+\nu}{E}\frac{\boldsymbol{\sigma}^\mu}{1-D} - \frac{\nu}{E}\frac{\mathrm{tr}\,\sigma^\mu}{1-D}\mathbf{1} + \alpha^\mu(T - T_{\mathrm{ref}})\mathbf{1} \tag{2}$$

where the thermal expansion coefficient α^μ is taken next equal to the meso coefficient α. In the yield criterion, the hardening X^μ is kinematic, linear, and the yield stress is the asymptotic fatigue limit of the material at $R\sigma = -1$, denoted σ_f^∞.

$$f^\mu = (\tilde{\boldsymbol{\sigma}}^\mu - \boldsymbol{X}^\mu)_{\mathrm{eq}} - \sigma_f^\infty \tag{3}$$

with $(.)_{eq}$ von Mises norm and where the elasticity domain is defined by $f^\mu<0$. The set of constitutive equations at microscale is then:

$$\begin{cases} \boldsymbol{\epsilon}^\mu = \boldsymbol{\epsilon}^{\mu e} + \boldsymbol{\epsilon}^{\mu p}, \\ \boldsymbol{\epsilon}^{\mu e} = \dfrac{1+\nu}{E}\tilde{\boldsymbol{\sigma}}^\mu - \dfrac{\nu}{E}\mathrm{tr}\,\tilde{\boldsymbol{\sigma}}^\mu\mathbf{1} + \alpha(T - T_{\mathrm{ref}})\mathbf{1}, \\ \dot{\boldsymbol{\epsilon}}^{\mu p} = \dfrac{3}{2}\dfrac{\tilde{\boldsymbol{\sigma}}^{\mu D} - \boldsymbol{X}^\mu}{(\tilde{\boldsymbol{\sigma}}^\mu - \boldsymbol{X}^\mu)_{\mathrm{eq}}}\dot{p}^\mu, \\ \dfrac{\mathrm{d}}{\mathrm{d}t}\left(\dfrac{\boldsymbol{X}^\mu}{C_y}\right) = \dfrac{2}{3}\dot{\boldsymbol{\epsilon}}^{\mu p}(1-D), \\ \dot{D} = \left(\dfrac{Y^\mu}{S}\right)^s \dot{p}^\mu \quad \text{if}\, p^\mu > p_D^\mu \text{ or if } w_s^\mu > w_D, \\ D = D_c \rightarrow \text{crack initiation} \end{cases} \tag{4}$$

with the plastic modulus C_y, the damage strength S, the damage exponent s as temperature dependent material parameters.

In previous laws, p^μ is the accumulated plastic strain at microscale, w_s^μ is the stored energy density and p_D^μ and w_D are the corresponding damage thresholds. A damage threshold in terms of accumulated plastic strain is loading dependent so that a threshold in terms of stored energy can advantageously be considered. A crack is initiated when D reaches the critical damage D_c.

3.5. Localization law coupled with damage and temperature

The scale transition meso to micro is governed by modified Eshelby-Kröner localization law [32, 33, 43]:

$$\varepsilon^{\mu D} = \frac{1}{1-bD}[\varepsilon^D + b((1-D)\varepsilon^{\mu p} - \varepsilon^p)] \tag{5}$$

$$\varepsilon_H^\mu = \frac{1}{1-aD}[\varepsilon_H + a((1-D)\alpha^\mu - \alpha)(T - Tref)] \tag{6}$$

Where $(.)^D=(.)-(1/3)tr(.)\mathbf{1}$ stands for the deviatoric part of a tensor, $(.)_H=(1/3)tr(.)$ for the hydrostatic part. By considering $\boldsymbol{\varepsilon} = \boldsymbol{\varepsilon}^D + \varepsilon_H\mathbf{1}$, $\varepsilon^{\mu D} + \varepsilon^\mu_H\,\mathbf{1}$ the localization law reads:

$$\varepsilon^\mu = \frac{1}{1-bD}\left[\varepsilon + \frac{(a-b)D}{3(1-aD)}tr\varepsilon 1 + b((1-D)\varepsilon^{\mu p} - \varepsilon^p)\right] + \frac{a((1-D)\alpha^\mu - \alpha)}{1-aD}(T - Tref)1 \tag{7}$$

with a and b the Eshelby parameters for a spherical inclusion.

$$a = \frac{1+\nu}{3(1-\nu)}, \quad b = \frac{2}{15}\frac{4-5\nu}{1-\nu} \tag{8}$$

3.6. Fatigue post-processor

The equations of the two-scale damage model were first implemented in a fatigue post-processor DAMAGE 2005 [37]. This post-processor is a FORTRAN program which explicitly solves the two-scale damage model constitutive equations with an Euler backward scheme but with no iteration at each time step (due to the linear feature of the kinematic hardening). A graphical interface makes the software use quite easy. For a given material parameters file and for a given loading sequence, the program calculates the time to crack initiation, i.e. the time to reach the critical damage D_c. The inputs are either 1D or come from any 3D behaviour tests and Finite Elements computations.

4. PHASE 1: EVALUATION

4.1. Tests and computation

The model, as formulated here-above was first evaluated by Snecma on a batch composed of 21 notched specimens of a titanium alloy at low temperature under constant amplitude and constant frequency high cycle fatigue loadings. 2D axisymmetric finite element computations were carried out using a simple isotropic hardening behaviour law only computed on one loading cycle (Fig. 3). Three notch geometries were modelized and tested: Kt = 1.5, 2.5 and 3 (where Kt stands for the stress concentration factor). The specimens height is 60 mm, their top diameter is 6 mm. Localized plastification can appear at the surface of the notch.

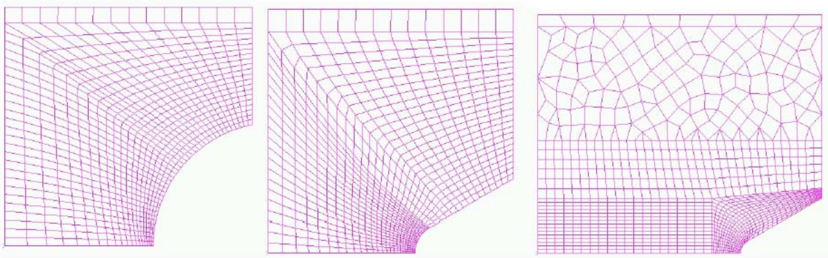

Figure 2: Details of the meshes in the notch for Kt = 1.5 (left) Kt = 2.5 (middle) and Kt = 3.5 (right).

The loading is presented in Fig. 3. It consists in an uniaxial (longitudinal) applied load varying between a maximum load F_{max} and a minimum load F_{min}. Different maximum loads were considered, corresponding to different numbers of cycles to crack initiation. Different positive load ratios $R_F = F_{min} / F_{max}$ were also considered, they were equal to the (applied) far field stress ratio and to the local longitudinal stress ratio $\sigma_{min}/\sigma_{max}$ obtained in elastic computations. Plastification took place in the stress concentration zone during the first load application (stage therefore called pre-plastification) making the local stress ratio R_σ obtained in plasticity different from the applied load ratio R_F (R_σ is in fact obtained lower than R_F).

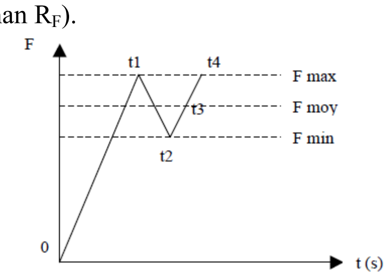

Figure 3: Applied loading

4.2. Results

As far as the unbroken specimens at 10^7 cycles were concerned, the model correctly announced the non-initiation of a crack in 10 cases out of 12 (83%). The mean factor 2 obtained between experimental break and previsions was quite a good result and corresponded to the expected performance of a life duration model in an industrial context. What was also of utmost importance at this stage was the ability of the model to correctly predict the time to crack initiation of specimens submitted to a high mean stress effect, with more or less yielding (up to 5% here) and for a multiaxial state of stress.

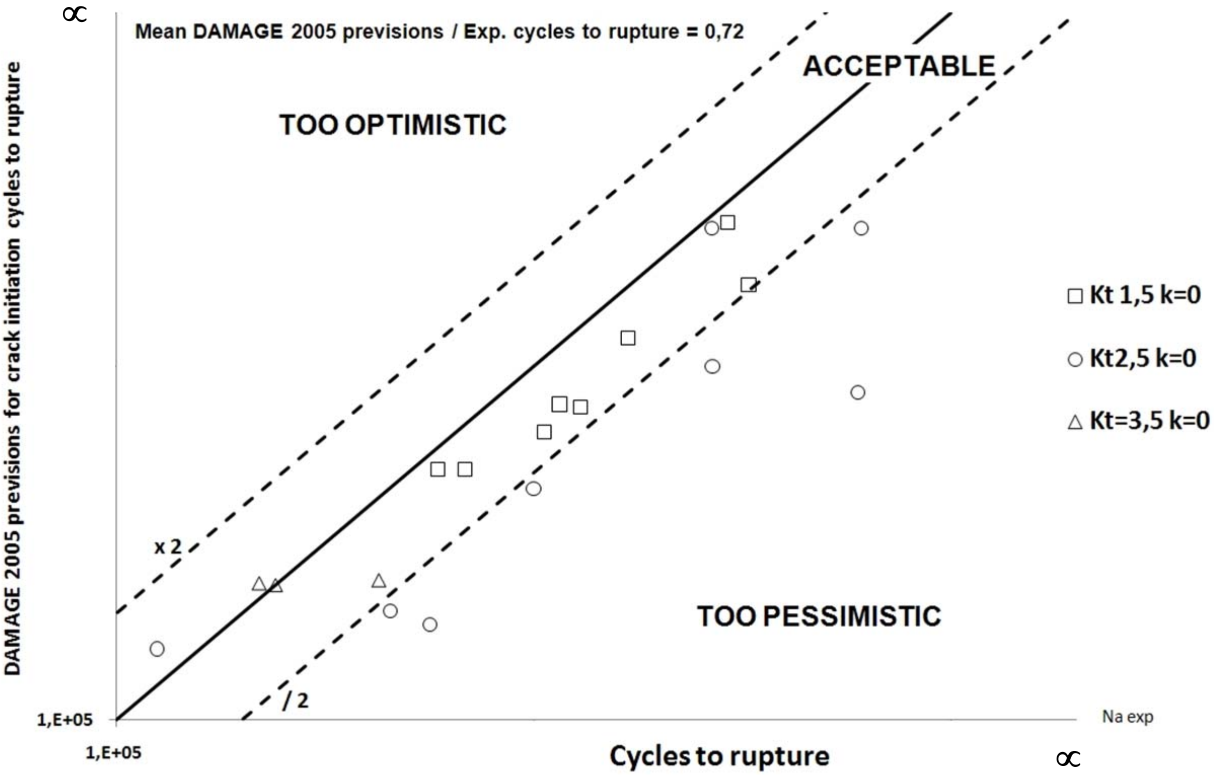

Figure 4: Comparison of experimental and predicted fatigue lives on broken notched specimens with DAMAGE 2005

But, to better visualize the results, they were plotted in a multiaxial Haigh diagram shown hereafter on Fig. 5 associated to the experimental and theoretical (i.e. given by the model) iso-life lines to crack initiation. Theoretical iso-life lines correspond to the model's response when stress ratio R_σ evolves from -1 to positive values.

The asymptotic fatigue limit is denoted $\sigma_f^\infty @ R_\sigma = -1$. The unbroken specimens after 10^7 cycles are represented by white marks whereas the broken ones are plain black. The smooth specimens ($R_\sigma = 0.1$) are represented by triangular marks. The notched specimens are represented by diamonds marks. As for notched specimens the state of stress is 3D, the octahedral shear A_{II} is plotted on the vertical axis.

$$\sigma_a = A_{\mathrm{II}} = \frac{1}{2}\sqrt{\frac{3}{2}(\boldsymbol{\sigma'}_{Max} - \boldsymbol{\sigma'}_{min}) : (\boldsymbol{\sigma'}_{Max} - \boldsymbol{\sigma'}_{min})} \tag{9}$$

On the horizontal axis, the trace of the mean stress tensor, is plotted.

$$\mathrm{tr}\,\overline{\boldsymbol{\sigma}} = \overline{\sigma}_{11} + \overline{\sigma}_{22} + \overline{\sigma}_{33} \quad \text{with} \quad \overline{\boldsymbol{\sigma}} = \frac{1}{2}(\boldsymbol{\sigma}_{min} + \boldsymbol{\sigma}_{Max}) \tag{10}$$

This representation offers the advantage to better take the stress triaxiality into account (it is consistent with Sines approach of multiaxial fatigue (Sines, 1959)). The further values of the trace of stress tensor are those of the smooth and notched fatigue specimens, computed by Finite Elements.

The horizontal line $A_{\mathrm{II}}/\sigma_f^\infty = \sigma_a/\sigma_f^\infty = 1$ or $A_{\mathrm{II}} = \sigma_a = \sigma_f^\infty$ corresponds to the infinite alternated fatigue limit in the 2005 release of the model. It is interesting to notice that, in this initial 2005 formulation, the frontier between broken and unbroken specimens is horizontal.

This point was not acceptable for most metallic materials which can be more sensitive to the mean stress effect.

So, in this initial version of the two-scale model, the predicted “no crack area” was a rectangular-shaped one as shown on the graph below:

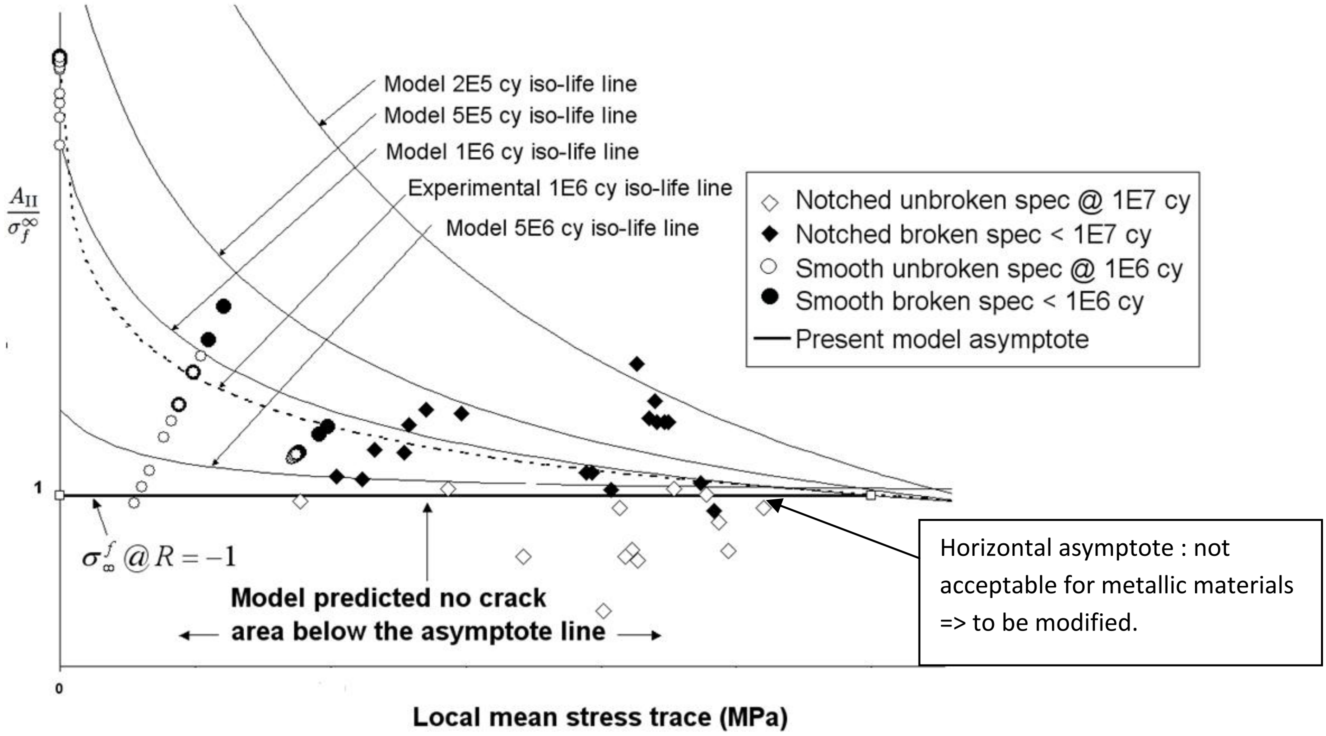

Figure 5: Multiaxial A_{II} vs $Tr(\underline{\underline{\sigma}})$ Haigh diagram for a titanium alloy at low temperature. Previous two-scale model formulation (2005) (before improvement).

In Figure 5 three different iso-lifetime lines predicted by the former version of the two-scale damage model have been plotted: the 5.10^5 (5E5), 1.10^6 (1E6) and 5.10^6 (5E6) iso-lifetime lines, with the corresponding experimental points. Several fatigue tests carried out on smooth specimens at $R_\sigma = -1$, $R_\sigma = 0.1$ and $R_\sigma = 0.5$ until 10^6 cycles allow to confirm the shape of $N_R = 10^6$ cycles line.

Remark that the model theoretical iso-lifetime lines sketched here are rapidly decreasing in the -1 to 0.1 R_σ range. All lines converge towards the asymptotic fatigue limit identified at $R_\sigma = -1$ (horizontal line $\sigma_a/\sigma_f^\infty = 1$). This line constitutes an asymptote for the iso-lifetime lines when the number of cycles to crack initiation increases. This feature is due to the fact that the asymptote has for equation $f^\mu = 0$ and that in the present case a von Mises plasticity criterion is considered at the microscale.

Let us insist once again on the fact that observations made here only concern locally plastified specimens. It wouldn't have been possible to explore such high stress ratio values and such high plastification levels in High Cycle Fatigue with smooth specimens.

4.3. Needs for improvements

This first evaluation study of the 2005 formulation of the two-scale model using the DAMAGE 2005 post-processor did put into relief the following points:

- Accuracy obtained on a batch of 21 notched specimens of a titanium alloy at different stress ratios R_σ at low temperature was rather satisfactory: a factor 2 was observed between experiments and theory.
- The fact that the fatigue limit was considered as unique whatever the stress ratio is, was not satisfactory. The way the mean stress effect was taken into account had to be improved.

5. PHASE 2: MODEL’S IMPROVEMENTS (2006-2009).

Uniaxial mean stress is defined as $\sigma_m = (\sigma_{min} + \sigma_{max}) / 2$ and is of course related to the stress ratio $R_\sigma = \sigma_{min} / \sigma_{max}$. It is observed that for negative mean stress, damage evolution is smaller than for positive mean stress. Taking this effect into account is important, especially for high mean stress loadings. Two main causes responsible for this effect are presented next.

5.1. Micro defects closure parameter "h"

So far, a difference between positive or negative mean stress loadings (and, as a consequence, between positive and negative stress ratios) was introduced in the two-scale model by the modelling of microdefects (or microcracks) closure by means of a microdefects closure parameter h in the expression of the energy density release rate:

$$Y^{\mu} = \frac{1+\nu}{2E}\left[\frac{\langle\boldsymbol{\sigma}^{\mu}\rangle^{+} : \langle\boldsymbol{\sigma}^{\mu}\rangle^{+}}{(1-D)^2} + h\frac{\langle\boldsymbol{\sigma}^{\mu}\rangle^{-} : \langle\boldsymbol{\sigma}^{\mu}\rangle^{-}}{(1-hD)^2}\right] - \frac{\nu}{2E}\left[\frac{\langle \mathrm{tr}\,\boldsymbol{\sigma}^{\mu}\rangle^2}{(1-D)^2} + h\frac{\langle -\mathrm{tr}\,\boldsymbol{\sigma}^{\mu}\rangle^2}{(1-hD)^2}\right] \quad (11)$$

$\langle\sigma^{\mu}\rangle^{+}$ and $\langle\sigma^{\mu}\rangle^{-}$ respectively denote the positive and negative parts of the stress tensor (in terms of principal values), $\langle x\rangle^{+}$ stands for the positive part of the scalar x, $\langle x\rangle^{+}$ = max(x, 0) (for metals h ≈ 0.2 [18, 34]) . In Fig.6, different values of "h" are plotted in a Haigh diagram ($\sigma_{alt}=f(\sigma_m)$) [44] with $\sigma_{alt} = 0.5\ \sigma_{max}\ (1- R_{\sigma})$) for a steel at 10^7 cycles. If h = 1, there is no mean stress effect, and if h = 0.2, there is a difference between positive and negative mean stress.

Comparing the Goodman line (with the coordinates (0, σ_f), (σ_u, 0)) [45] valid for unixial loadings (smooth fatigue specimen) we can see a gap between lines with "h" and the Goodman line for high stress ratios. We can experimentally observe that in function of the stress ratio level, the stress confinement in the loading (or plastified) zone and the multiaxiality of local stresses, that the parameter "h" could not be enough to represent real behaviour of materials.

So, it was necessary to go further into the modelization of the mean stress effect.

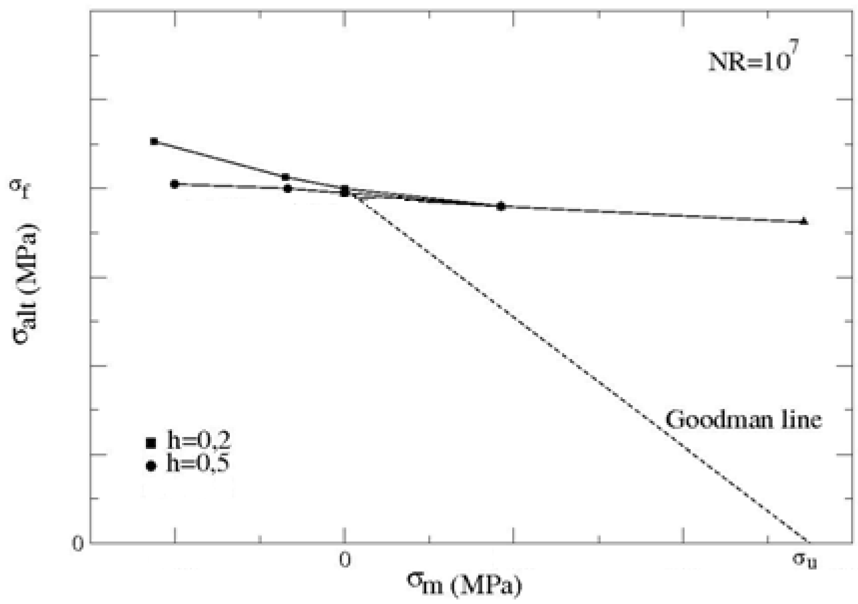

Figure 6: - Influence of the micro-defects closure parameter h on a Haigh diagram – 304L application.

5.2. Implementation of a Drucker-Prager term

In geomaterials, it is usual to introduce the Drucker-Prager yield criterion [41] (first stress invariant in the yield function) to reproduce cohesive properties of materials. Assuming here that the imbedded inclusion has a confined behavior, the yield function at microscale is so modified by adding the first stress invariant:

$$f^{\mu} = (\tilde{\sigma} - X^{\mu})_{eq} + kTr\tilde{\sigma}^{\mu} - \sigma_f^{\infty} \quad (12)$$

with Tr(.) the first stress invariant of the stress at micro scale, and k a Drucker-Prager parameter to identify.

5.3. Influence of parameter "k"

By time integration of the constitutive equations for a proportional loading in tension compression, we obtain the expression of the number of cycles to rupture $N_R = N_R(D = D_c)$ when the damage D reaches the critical damage D_c. The denominator of this expression can be written as: $\sigma - 2\sigma_f^{\infty} + 2\ k\ \sigma_m$.

The asymptotic fatigue limit corresponding to an infinite number of cycles to rupture is obtained for $\sigma - 2\sigma_f^{\infty} + 2\ k\ \sigma_m = 0$ and corresponds to an asymptote of the Wöhler curve. By keeping in mind the definition of a Haigh diagram ($\sigma_{alt} = f(\sigma_m)$) we obtain the expression of the asymptotic fatigue limit: $\sigma_{alt} = \sigma_f^{\infty}$-k σ_m. In a Haigh diagram, k is the slope of the asymptotic limit which delimits infinite lifetime from finite lifetimes.

A Haigh diagram is computed using DAMAGE 2010 post-processor for smooth specimen (Fig. 7). Cases k = 0 and k ≠ 0 are compared. Asymptotic fatigue limit (bold lines) and lines at $N_R = 1.10^6$ cycles (thin lines) are plotted.

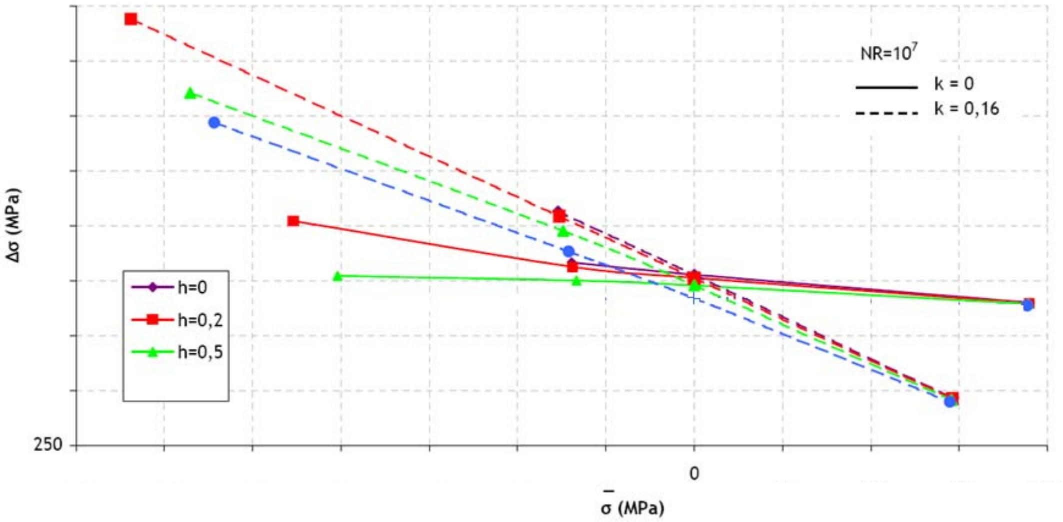

Figure 7: - Influence of h with or without consideration of the first stress invariant (k=0.16 or k=0) for a given number of cycle to rupture. Application to AISI 304L steel.

We can observe that:

- - for k = 0, the asymptotic limit in the Haigh diagram is a horizontal line. For a high mean stress loading, corresponding to a point below this asymptotic limit, the post processor will always find an infinite lifetime.
- - for k ≠ 0, the asymptotic limit in the Haigh diagram is a line with a negative slope. This property allows for the points corresponding to high mean stresses to have a finite lifetime.

During his Ph-D work, Barbier established [42] that with this modification, the model becomes equivalent, for infinite fatigue life, to the Sines criterion.

The Sines fatigue criterion is based on phenomenological considerations and uses the octahedral shear A_{II} (9) and the mean value of the hydrostatic stress. The Sines criterion predicts the appearance of a crack initiation when the equation below is satisfied:

$$A_{II} - \sigma_f (1 - 3b\bar{\sigma}_H) = 0 \qquad (13)$$

It is demonstrated ([42] and [46]) that parameter k is equivalent to the term "$b\sigma_f$" of the Sines criterion below.

6. PHASE 3 : MODEL'S VALIDATION.

6.1. Notched specimens

Once modified as presented before it was then possible to test the new model on the same batch of notched titanium alloy fatigue specimen (cf. §4). The results are shown hereafter.

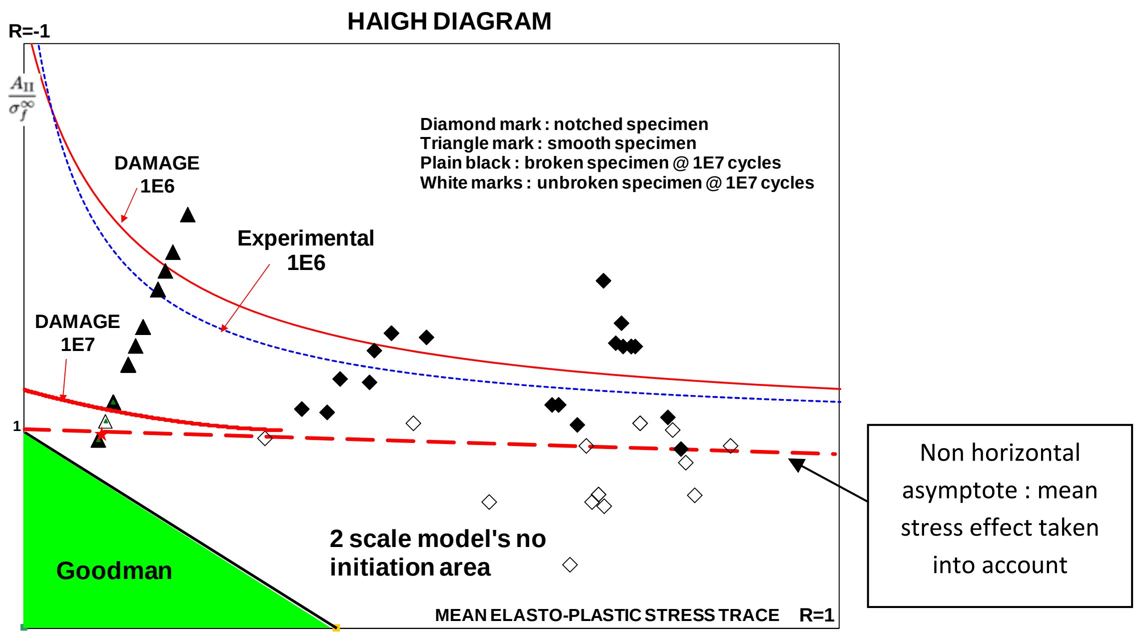

Figure 8: Multiaxial A_{II} vs $Tr(\underline{\underline{\sigma}})$ Haigh diagram for a titanium alloy at low temperature. New two-scale model formulation (2010) with Drucker-Prager improvement.

It can be seen on this graph that thanks to the improvements, 100% of the broken specimen are predicted as such thanks to the non horizontal asymptote of the model ($k = e \neq 0$).

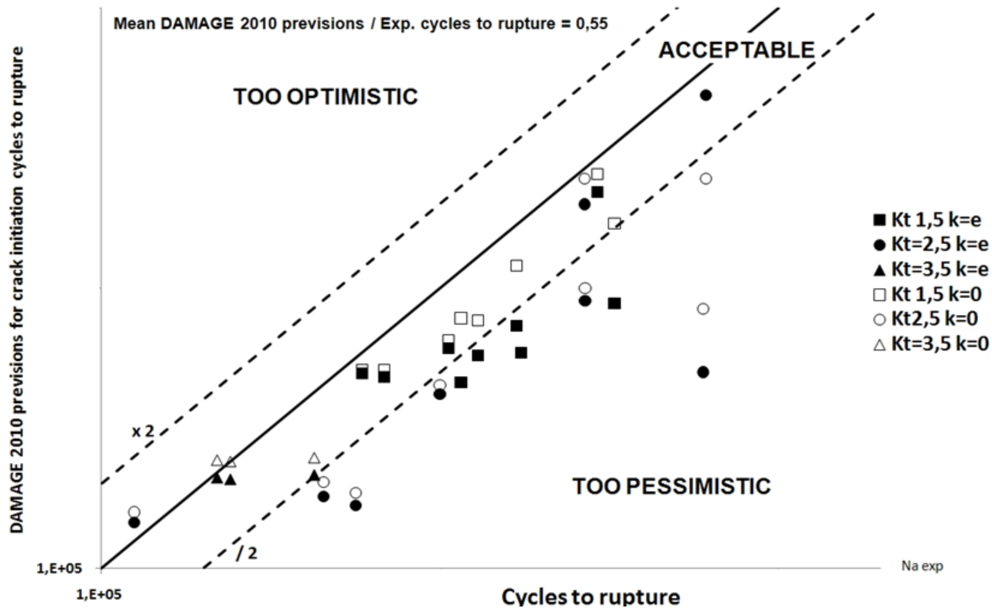

Figure 9: Comparison of experimental and predicted fatigue lives on broken notched specimens with DAMAGE 2010

Initiation predictions are slightly modified in comparison to those shown on Fig. 4 : they are more pessimistic here for this alloy but the mean ratio between predictions and experimental cycles to rupture remain very satisfactory (0.55). For other metallic alloys (Ni based) studied but not presented here, the results obtained with the new release of DAMAGE are greatly improved as far as non rupture and initiation prevision are concerned.

For specimens with cycles to rupture lower than 1E5, previsions are even better with the k slope of DAMAGE 2010. Nevertheless, the predictive efficiency remains poor in LCF since the model is basically written for HCF.

6.2. Biaxial fatigue tests

Another way to validate the model was to use it to predict the crack initiation of thinned Maltese cross shaped specimen submitted to high stress ratios.

Biaxial tests on titanium alloy Maltese cross specimen have thus been carried out on LMT Cachan test facility ASTREE. This testing machine has six servohydraulic actuators. The four horizontal actuators used herein have a 100 kN load capability and a 250 mm stroke range. The Maltese cross specimen has been designed (Fig.10) thanks to Finite Element Cast3m code and DAMAGE 2005 post-processor by Barbier, Desmorat and du Tertre (2006). This specimen is made to initiate HCF crack in its central area under various (proportional, non proportional) biaxial loadings.

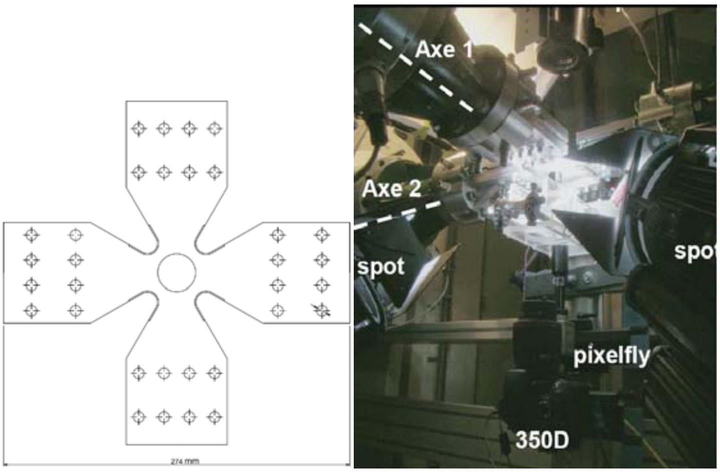

Figure 10 : a) Geometry of the specimen. b) General view of a biaxial test.

Biaxial tests were load controlled and performed at room temperature. The test frequency was 20Hz. Even if the permanent strains in central area are very small, digital image correlation was used to have the strains fields in the entire specimen and not only on a small zone corresponding to a gauge.

Strain fields are monitored using different cameras. Eight biaxial tests were performed, different kinds of experimental set up were tested.

Eight tests are presented here (represented by a letter going form A to H). Tests could be divided into three kinds of various loadings :

- Tests A and B correspond to equibiaxial tests (in phase) at two different load ratios. (RF=0.1 for test A, RF=0.5 for test B).
- Test C, D, E, F and G are non equibiaxial tests (in phase) with different load ratios on each direction.
- Test H corresponds to 90° out of phase non equibiaxial test with different load ratio on each direction.

Table 1 – Tests summary

test	C, D	E	F	G
R_F direction 1	0.5	0.6	0.4	0.1
R_F direction 2	0.4	0.5	0.3	1.0 (F=cste)

As previously described, the maximum strain amplitude loading is defined to compare biaxial and uniaxial tests. Figure 11 represents fatigue results of biaxial tests and uniaxial tests performed at a load ratio of R_F=0.1 (test C presented a machining irregularity in the central area which led to a shorter life than expected).

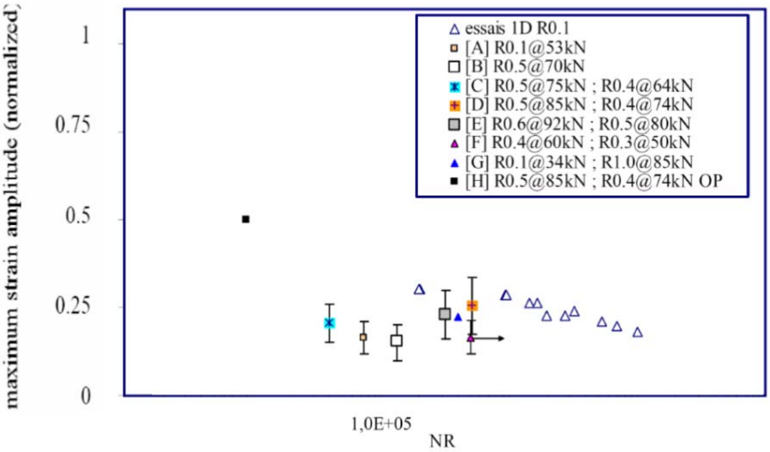

Figure 11. : Summary of biaxial fatigue results for titanium alloy (A, B, C and F tests specimen geometries are thicker).

As all these tests were performed at different load ratios, with different applied forces, it is quite difficult to compare them. Anyway, with the proposed representation of results, one can observe that :

- D versus H tests : out of phase effect under the same loading. For out of phase loading, the maximum strain amplitude is about twice as the in-phase corresponding loading. The number of cycles for the out of phase loading is 40 times less than the in-phase loading.

- Multiaxial tests, even if performed at different load ratios R_F than uniaxial tests (1D tests @ $R_F = 0.1$), are all located beneath these ones : one can observe here the negative aspect of multiaxiality on the fatigue life.

The comparison between predicted and experimental number of cycles is shown here-after :

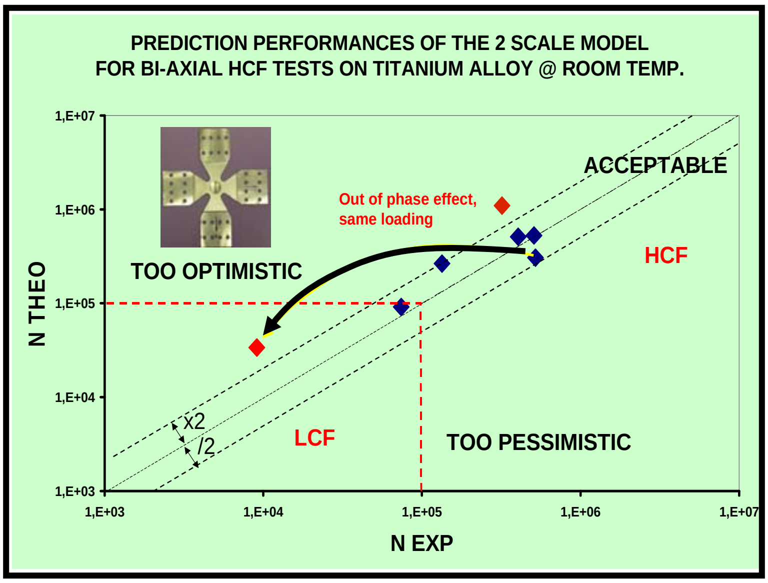

Figure 10. : Comparison between predicted and experimental values for titanium alloy (DAMAGE 2010 release).

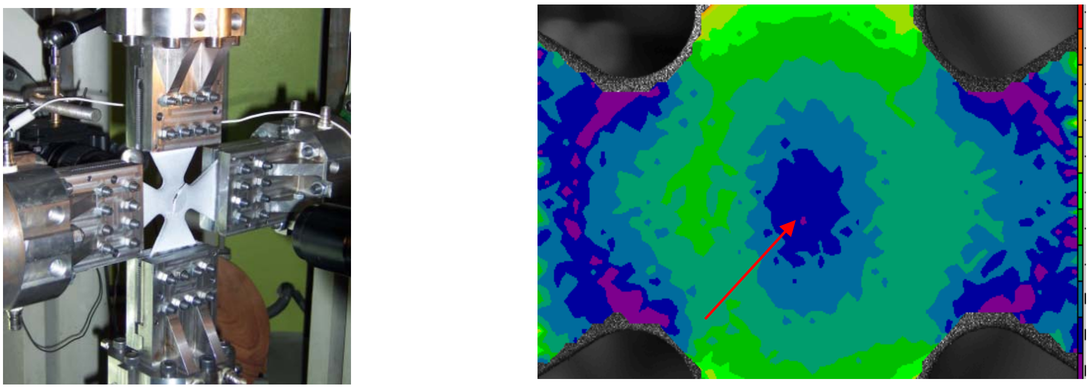

a) **b)**

Figure 11 - a) View of the specimen during test. b) Strains fields obtained by image correlation (Correli LMT). Titanium alloy.

Central fatigue crack initiation was clearly established thanks to LMT Correli strain fields analysis software which uses image correlation techniques.

7. CONCLUSION

Since 2005 the studies carried out in cooperation between Snecma and the LMT but also other industrial partners allowed to evaluate the predictive performances of the two-scale model on different materials (Fe, Ti, Ni alloys) and to propose improvements, especially in the way the mean stress effect is taken into account.

Thanks to the introduction of a Drucker-Prager term in the yield function of the model, the corresponding post-processor DAMAGE is now able to better take into account this mean stress effect in a wide stress ratio range. The identification of the Drucker-Prager parameter is simple, and is function of the stress ratio of the experimental Wöhler curve. This parameter k has a physical meaning: it is the slope of the asymptotic limit in a Haigh diagram. Thanks to this parameter, it is now possible to more precisely represent the behavior of real specimen under HCF loadings.

Moreover, it has been established that this modification of the yield function at microscale leads to a Sines equivalent crack initiation criterion.

A validation test campaign performed on smooth and notched uniaxial specimens but also on 8 bi-axial titanium alloy specimens at high stress ratios finally allowed to validate the improvements introduced. A factor 2 can globally be observed between experimental and numerical number of cycles to rupture.

Validation process will now go on by exploring other aspects which will lead to other possible developments.

8. ACKNOWLEDGMENTS

Snecma and LMT-Cachan would like to especially acknowledge CNES (Direction des Lanceurs) for its support of this study.

9. REFERENCES

1 Basquin, O.H., 1910. The exponential law of endurance tests. Proc. ASTM, 10, 625-630.
2 Manson, S.S. and Hirschberg, M.H., 1964. Fatigue: An Interdisciplinary Approach. Syracuse University Press, Syracuse, N.Y.
3 Aas-Jackobsen K., Lenshow R., Behavior of reinforced columns subjected to fatigue loading, ACI Journal, 70(3), pp. 199-206, 1973.
4 Leiholz H. H. E., On the modified S-N curve for metal fatigue prediction and its experimental verification, Engineering Fracture Mechanics, vol.23, pp. 495-505, 1986.
5 Fatemi A., Yang L., Cumulative fatigue damage and life prediction theories: a survey of the state of the art for homogeneous materials, International Journal of Fatigue, vol. 20, pp. 9-34, 1998.
6 Smith R., Watson P., Topper T., A stress-strain function for the fatigue of metals. Journal of Mat., vol. 5, pp. 767-778, 1970.
7 Brown M.W., Miller K.J., A theory for fatigue failure under multiaxial stress-strain conditions. Institution of Mechanical Engineers, Proceedings. vol. 187, no. 65, pp. 745-755. 1973

8 Dang-Van K., Sur la résistance à la fatigue des métaux, Sciences et Techniques de l'Armement, vol. 3, pp. 647-722, 1973.
9 Hua, C.T. and Socie, D.F., Fatigue damage in 1045 steel under constant amplitude biaxial loading. Fatigue Eng. Mat. Struct., 7, 165-179, 1984.
10 Dang-Van K., Macro-Micro Approach in High-Cycle Multiaxial Fatigue, Advances in Multiaxial Fatigue, ASTMSTP1191, D.L. McDowell and R. Ellis Eds., American Society for Testing Materials, Philadelphia, pp. 120-130, 1993.
11 Papadopoulos I. V., A high-cycle fatigue criterion applied in biaxial and triaxial out-of-phase stress conditions, Fatigue & Fracture of Engineering Materials & Structures vol. 18(1), pp. 79-91, 1995.
12 Papadopoulos I. V., Davoli P., Gorla C., Filippini M. and Bernasconi A., A comparative study of multiaxial high-cycle fatigue criteria for metals, International Journal of Fatigue Vol. 19(3), pp. 219-235, 1997.
13 [13] Nicholas T., Critical issues in high cycle fatigue, International Journal of Fatigue, 21(1), pp. 221-231, 1999.
14 Morel F., A critical plane approach for life prediction of high cycle fatigue under multiaxial variable amplitude loading. International Journal of Fatigue vol. 22(2), pp. 101-119, 2000.
15 Lemaitre J., Chaboche J.L., A non-linear model of creep-fatigue damage cumulation and interaction, Symposium IUTAM, Gothenburg, 2-6 september 1974.
16 Lemaitre J., Plumtree A, Application of damage concepts to predict creep fatigue failures, Journal of Engineering Materials Technology, vol. 101, pp. 284-292, 1979.
17 Chaboche J.L., Lesne P.M., A non-linear continuous fatigue damage model, Fatigue Fracture Engng Mater Struc 11, 1-17, 1988.
18 Lemaitre J., A course on damage mechanics, Springer Verlag, 1992.
19 Paas, M.H., Schreurs, P.J.G. and Brekelmans, W.A.M., A continuum approach to brittle and fatigue damage: theory and numerical procedures. Int. J. Solids Struct., 30, 579-599, 1993.
20 Desmorat R., Damage and fatigue: continuum damage mechanics modeling for fatigue of materials and structures, Revue Européenne de Génie Civil, 10, p. 849-877, 2006.
21 Flacelière L., Morel F., Dragon A., Coupling Between Mesoplasticity and Damage in High-cycle Fatigue, International Journal of Damage Mechanics, 16, pp. 473-509, 2007.
22 Ladevèze P., Lemaitre J., 1984, Damage effective stress in quasi unilateral conditions, 16th International Congress of Theoretical and Applied Mechanics, Lyngby, Denmark.
23 Chaboche, J.L., Development of continuum Damage Mechanics for elastic solids sustaining anisotropic and unilateral damage, Int. J. Damage Mechanics, Vol. 2, pp. 311-329, 1993.
24 Desmorat R., Ragueneau F., Pham H., Continuum Damage Mechanics for hysteresis and fatigue of quasi-brittle materials and structures, International Journal of Numerical and Analytical Methods for Geomaterials, vol. 31, p. 307-329, 2007.
25 Desmorat R., Cantournet S., Modeling micro-defects closure effect with isotropic/anisotropic damage, International Journal of Damage Mechanics, vol. 17, pp. 65{96, 2008.
26 Lemaitre J., Doghri I., Damage 90: a post-processor for crack initiation. Comp. Methods Appl. Mech. Engrg. 115: 197-232, 1994.
27 Lemaitre J., Sermage J.P. , Desmorat R., A two-scale damage concept applied to fatigue, International Journal of Fracture, vol. 97, pp. 67-81, 1999.
28 Desmorat R., Lemaitre J., Two-scale damage model for quasi-brittle and fatigue damage, Handbook of Materials Behavior Models, J. Lemaitre Ed., Academic Press, chapter Continuous Damage, section 6.15, pp. 525-535, 2001.
29 Desmorat R., Kane A., Seyedi M., Sermage J.P., Two-scale damage model and related numerical issues for thermo-mechanical High Cycle Fatigue, Eur. J. Mech A/Solids, Vol. 26, pp. 909-935, 2007.
30 Sauzay M., Effet de surface en fatigue polycyclique, PhD thesis Univ. Paris 6, 2000.
31 Lemaitre, J., Chaboche, J. L., Mécanique des matériaux solides, Dunod 1985, Mechanics of solid materials, Oxford University Press, 1991 (English translation).
32 Eshelby J.D., The determination of the elastic field of an ellipsoidal inclusion, related problems, Proc. Roy. Soc., London, vol. A241, p. 376, 1957.
33 Kröner E., On the plastic deformation of polycrystals, Acta Metall., vol. 9, pp. 155-161, 1961.
34 Lemaitre J., Desmorat R., Engineering Damage Mechanics : Ductile, Creep, Fatigue and Brittle Failures, Springer, 2005.
35 Sermage J. P., Lemaitre J., Desmorat R., Multiaxial creep fatigue under anisothermal conditions, Fatigue and Fracture of Engng Mater. & Struct., 23(3), pp. 241 - 252, 2000.
36 François D., Pineau A., Zaoui A., Comportement mécanique des matériaux en élasticité et plasticité, Hermes Paris, 1992.
37 Desmorat R., Pauget F., Sermage J.P., DAMAGE 2005: a post-processor for High Cycle Fatigue under complex thermomechanical loading, ASME Pressure Vessels and Piping Division Conference, Vancoucer, BC, Canada, july 23-27, 2006.

38 Lanning D. B., Nicholas T., Haritos G.K., On the use of critical distance theories for the prediction of the high cycle fatigue limit stress in notched Ti-6Al-4V, International Journal of Fatigue, vol. 27, pp. 45-57, 2005.
39 Sines, G., Behavior of metals under complex static and alternating stresses. In: Sines, G., Waisman, J.L. (Eds.). McGraw-Hill, New York, pp. 145-169, 1959.
40 Desmorat R. et al. 2007. Two-scale damage model and related numerical issues for thermo-mechanical High Cycle Fatigue, Eur. Jour. of Mech. A/Solids, Vol. 26, pp. 909-935.
41 Drucker D. C. and Prager W., Soil Mechanics and Plastic Analysis of Limit Design, Quart. Applied Mathematics, Vol.10, No.2, 1952.
42 Barbier. G. Ph-D Thesis. Fatigue biaxiale à grand nombre de cycles : étude expérimentale et modèle à deux échelles probabiliste. LMT Cachan; ENSC-2009n°208 ;14/12/2009.
43 Seyedi, M., Desmorat, R., Sermage, J.-P., A two-scale model for thermo-mechanical high cycle fatigue failure. In: European Conference on Fracture ECF 15, Advanced Fracture Mechanics for Life and Safety, Stockholm, Sweden, 2004.
44 Haigh BP. Experiments on the fatigue of brasses. J Inst Metals;18:pp.55–86, 1917.
45 Goodman J. Mechanics applied to engineering. 1st ed. London: Longmans, Green and Co., 1899.
46 du Tertre A., Barbier G., Desmorat R., Sermage J.-P., Courtin S; Mean stress effect from Drucker-Prager micro-plasticity criterion, EUCASS conference 2009; 6-9th july 2009. Versailles.